02,19

Superconducting bolometer with high-frequency readout circuit at 400 mK

© A.V. Merenkov, T.M. Kim, V.I. Chichkov, S.V. Kalinkin, S.V. Shitov

National University of Science and Technology MISiS,
Moscow, Russia

E-mail: merenkov.alexey92@gmail.com

Received April 29, 2022
Revised April 29, 2022
Accepted May 12, 2022

The detection of a terahertz optical signal using a bolometric detector with a planar niobium resonator loaded with a hafnium micromotor using the nonlinearity of the impedance of an electron gas at a frequency of 1.5 GHz near the critical temperature of the micromotor is demonstrated for the first time. The temperature of the electron gas was shifted by the resonator current, and the superconducting transition of the micromotor occurred under the action of a terahertz signal. The test thermodynamic signal from a thin-film Fe-Cr-Ni absorber heated in the range of $1-10$ K was focused from a distance of 10 mm with an immersion lens made of sapphire onto a planar antenna matched with a micro-bridge in the range of $600-700$ GHz. The measured power transmission coefficient of the bolometer was $+5.5$ dB with a saturation power of ~ 1 pW and a threshold sensitivity of the receiving system $(3 \pm 1) \cdot 10^{-17}$ W/$\sqrt{\text{Hz}}$ sqrt, which is close to the theoretical values for the investigated bridge with a size of $2.5 \times 2.5 \times 0.08\,\mu$m. The tested detector can be used to create imaging terahertz matrices with frequency multiplexing in sorption-type cryostats. Keywords: RFTES bolometer, superconducting micro bridge, high-frequency impedance of superconductor, hafnium film, electron gas, planar resonator, frequency multiplexing, planar antenna, black body, thermodynamic noise.

Keywords: RFTES bolometer, superconducting microbridge, high-frequency impedance, hafnium film, electron gas, coplanar resonator, frequency-division multiplexing, planar antenna, blackbody, noise.

DOI: 10.21883/PSS.2022.10.54223.50HH

1. Introduction

Recently, there has been an upsurge in interest on the part of the astrophysical community in ultrasensitive imaging direct terahertz detectors based on superconducting materials, especially in the form of integrated arrays with a number of pixels of ~ 1000 [1–7], including those on orbital carriers. The monolithic detector proposed by us, which received the abbreviation RFTES (radio frequency transition edge sensor) [8–16], is a nonequilibrium thermal detector and retains the features of known superconducting detectors, having several advantages. The response of the detector is based on the high-frequency nonlinearity of the surface impedance of a superconductor [17], formed as a thin-film microbridge, included in a high-Q quarter-wave resonator. Under the influence of a terahertz current coming from a planar antenna, the temperature of the electronic subsystem of the superconductor rises near its critical temperature, and the circuit impedance increases. This leads to an increase in the transmission of the resonator circuit shown in Fig. 1, which in terms of circuit theory means an increase in the dissipation factor S_{21}. The RFTES bolometer got its name by analogy with the classic TES bolometer (transition edge sensor, i.e. sensor at the edge of a superconducting junction) [1,2]. The TES bolometer consists of an absorber-pad on a heat-insulating membrane in thermal equilibrium with a thermometer, i.e.with a superconductor film near T_c, changing its impedance as the absorber is heated by the signal.

The impedance of classical TES is small (units of Ω), and to measure it at a direct (low-frequency) current, galvanic leads are required, as well as an ultra-low-noise current amplifier, which is used as a superconducting SQUID amplifier. As follows from Fig. 1, the RFTES bolometer does not need galvanic connections; bias and buffer amplifier connections can be made with coaxial cables by standard $50\,\Omega$. This provides reliable protection against interference and increases the survivability of RFTES. Another difference is that the RFTES absorber and thermometer are combined in a small volume of a film deposited on a mechanically stable dielectric substrate, and heating occurs by the antenna current, which itself does not heat up. High-Q superconducting resonator ($Q \approx 2 \cdot 10^4$) is very sensitive to the appearance of additional losses and simultaneously serves as a frequency-selective filter. By tuning the pixel resonators to unique frequencies, a single bias line can be used for a large array. From the theory of oscillations, it is known that for a high-Q resonator under the influence of small current/voltage, the characteristic time of oscillation settling τ_R coincides with the characteristic decay time, which is determined by the Q-quality of this oscillatory system. The frequency band of the resonator, $\Delta f_R = f_R/Q$, is measured experimentally, which makes it possible to determine $\tau_R = \Delta f_R^{-1}$. Under the action of small signals, small changes in the Q-quality occur, which do not

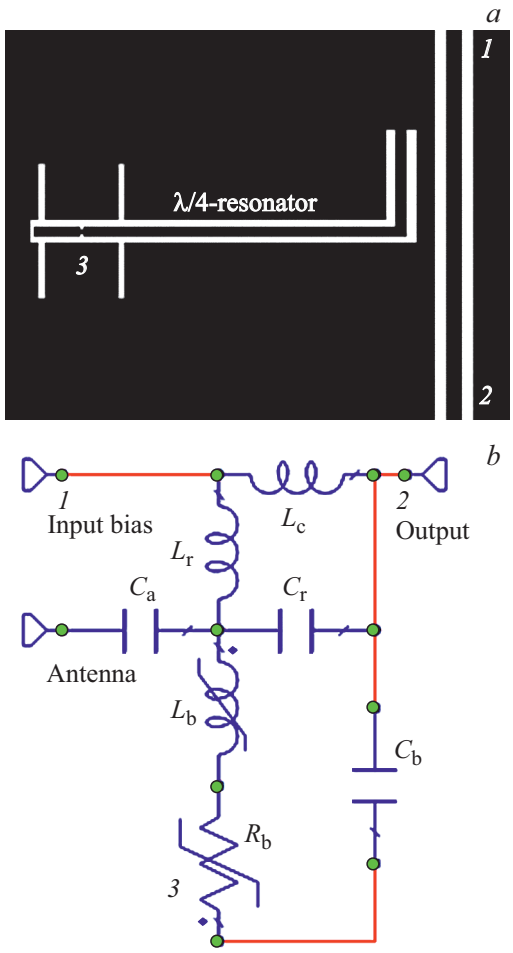

Figure 1. RFTES bolometer concept: *a*) RFTES topology illustration (not to scale, metal shown in black); *b*) simplified equivalent circuit: R_b is non-linear bridge impedance, L_b is kinetic bridge inductance, C_b is blocking capacitance, L_r and C_r are inductance and capacitance that determine the resonator frequency, L_c is coupling element of the resonator and the displacement line $L_c \ll L_r$. The numbers indicate: *1* and *2* are input and output of the line of the coplanar bias waveguide, *3* is microbridge matched simultaneously with the planar double-slot antenna in the range of 600−700 GHz and with a resonator at a frequency of ∼ 1.5 GHz.

exceed a few percent, and for a number of estimates such changes can be neglected. In practice, the minimum signal settling time is chosen no shorter than $(2-3)\tau_R$, which at the resonator frequency ∼ 1.5 GHz with a band ∼ 80 kHz is ∼ (25−38) μs. This is by more than 2 orders of magnitude faster than TES (∼ 10 ms).

The most important parameter of the bolometer is the thermal insulation of the absorber, which is not a trivial task in the case of a detector with monolithic structure. Electrodynamic prototypes of RFTES have been tested in experiments with niobium bridges at liquid helium temperatures (∼ 4 K) [9–12]. The correctness of the electrodynamic calculations was confirmed and the threshold sensitivity ∼ 10^{-12} W/$\sqrt{\text{Hz}}$, which corresponds to the Kapitza's thermal resistance was demonstrated. The purpose of further research of RFTES was to apply the electron gas effect similar to HEB (hot electron bolometer) [5–7]. Direct detectors based on hot electron gas become relevant at temperatures below ∼ 1 K, when the electron-phonon relaxation time becomes sufficiently long, and the thermal insulation between the electron subsystem and the lattice exceeds the Kapitza resistance by an order of magnitude. For the hafnium bridge considered in this work, the heating rate is determined by the time of heat distribution in the electronic subsystem, that is, the rate of electron-electron interaction: calculation by the methodology [18] gives ∼ 15 ns at temperature ∼ 400 mK. The cooling rate is determined by the electron-phonon relaxation time of the electron gas, ∼ 10 μs at temperature ∼ 400 mK, which agrees in order of magnitude with the resonator reaction time. The thermal conductivity G of the electron gas in the microbridge decreases in proportion to the decrease in its volume and in a power-law manner with decreasing temperature. Measurements at the frequency ∼ 1.5 GHz [14–16] showed that the thermal conductivity for our samples in the temperature range of 200−400 mK is $10^{-12}-10^{-11}$ W/K, and the temperature dependence is $G \propto T^5$. These data confirmed that it is the electron gas that is responsible for the heating and heat insulation in the bridge, and the Kapitsa resistance can be neglected. It should be noted that such a result would not have been possible without the presence of heat-insulating Andreev mirrors [19] in the contact area of the microbridge with niobium electrodes.

The threshold sensitivity of direct detectors is characterized by the universal parameter NEP (noise equivalent power), which is measured in W/$\sqrt{\text{Hz}}$ units for the output integrator bandwidth $f_{\text{out}} = 1$ Hz. For arbitrary band of the integrator, the threshold signal will be different, i.e. it is defined as NEP $\cdot \sqrt{f_{\text{out}}}$. This scaling of the threshold sensitivity is due to the properties of a quadratic detector; it allows to correlate the maximum rate of change of the signal and the level of its detection using the universal definition of NEP, which is relevant for any detector in fast signal mode.

Let's compare the potential of RFTES with t he existing and generally recognized leaders: with the HEDD (hot electron detector device) [20], which operates on direct current, and with the MKID (microwave kinetic inductance detector) [3,4], which uses high-frequency microresonators and a standard cooled microwave amplifier. The HEDD detector is positioned as a record sensor with NEP ≈ 10^{-20} W/$\sqrt{\text{Hz}}$ [20]. Frequency selective multiplexing of the MKID array is currently recognized as the most convenient technology for cooled array detectors, and NEP is ∼ 10^{-18} W$\sqrt{\text{Hz}}$ [3,4]. The advantages of RFTES can be considered the following: 1) RFTES is superior to HEDD in terms of performance, as it allows you to abandon the expensive and very delicate SQUID amplifier in tuning, and can also use frequency-selective multiplexing to build matrices; 2) RFTES retains the advantages of MKID

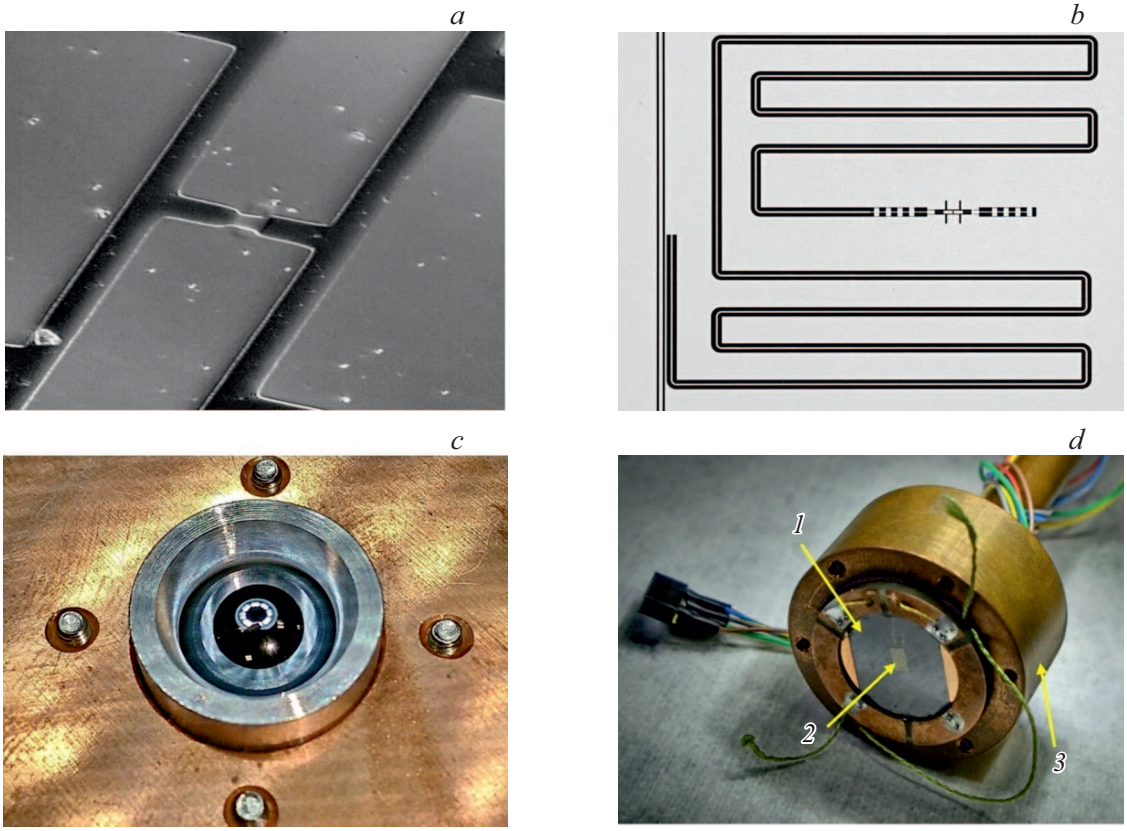

Figure 2. Detector elements and black-body emitter: *a*) microbridge in the center of the planar antenna; *b*) the central region of the chip with a folded quarter-wave resonator and a planar antenna; *c*) input aperture of the detector with immersion lens; *d*) test source of broadband radiation (black body): *1* is translucent resistive absorber film on a sapphire substrate; *2* is thermometer on the back side of the substrate; *3* is housing-holder $T \approx 1$ K).

frequency multiplexing and at the same time makes it possible to fundamentally reduce the influence of bias source phase noise, inevitable for MKID. The resonant frequency of the MKID shifts down under the action of terahertz photons, so the operating point is chosen on the slope of the resonant curve, where the derivative $dS_{21}(f)/df$ is maximal. Any bias generator has unremovable phase/frequency noise with amplitude Δf, this leads to amplitude noise of the output signal $\propto \Delta f \cdot dS_{21}(f)/df$. By contrast to this, the operating point of RFTES is located exactly at the resonant frequency, where $dS_{21}(f)/df|_{f_0} = 0$, i.e. a small change in frequency Δf (or phase jump) cannot be converted to amplitude noise in the manner described above. Electron-cooled detectors [7] seem to us to be much more complex in design, and it is difficult to compare them with RFTES.

In this work we present for the first time the results of RFTES detector testing with a thermodynamic signal source at detector temperature of 400 mK. Such a relatively high operating temperature will make it possible to use a cheaper sorption refrigerator in practice, which significantly reduces the technical complexity and operating cost of a practical receiving device, allowing it to be used, including under weightless conditions.

2. Experimental setup

The measurements were carried out in the temperature range of 390−410 mK in a DR-200 dilution refrigerator by Oxford Instruments. Sensing element i.e. hafnium microbridge (Fig. 2, *a*) $2.5 \times 2.5 \times 0.08\,\mu$m and normal resistance ~ 30 Ohm, is integrated into the discontinuity of a coplanar resonator made of niobium film with thickness of about 200 nm, so that it is connected simultaneously with the resonator current at frequency of ~ 1.5 GHz, and with the current of planar double-slot antenna in frequency range of 600−700 GHz, as illustrated in Fig. 1. The antenna is located in the center of a $4 \times 4 \times 0.5$ mm high-resistance silicon chip (Fig. 2, *b*). All elements were formed by optical lithography with an accuracy of no worse than $0.5\,\mu$m. The chip was mounted in the detector unit on flat surface of hemispherical sapphire immersion lens with diameter of 10 mm [21] (Fig. 2, *c*). More detailed description of the design and manufacturing procedure of the chip can be found in the works [12,13].

As a test thermodynamic oscillator, the thin resistive film (~ 1000 Ohm/kv) made of Fe-Cr-Ni alloy deposited by magnetron sputtering on a sapphire substrate 0.5 mm thick and 15 mm in diameter, was used. The calculation showed

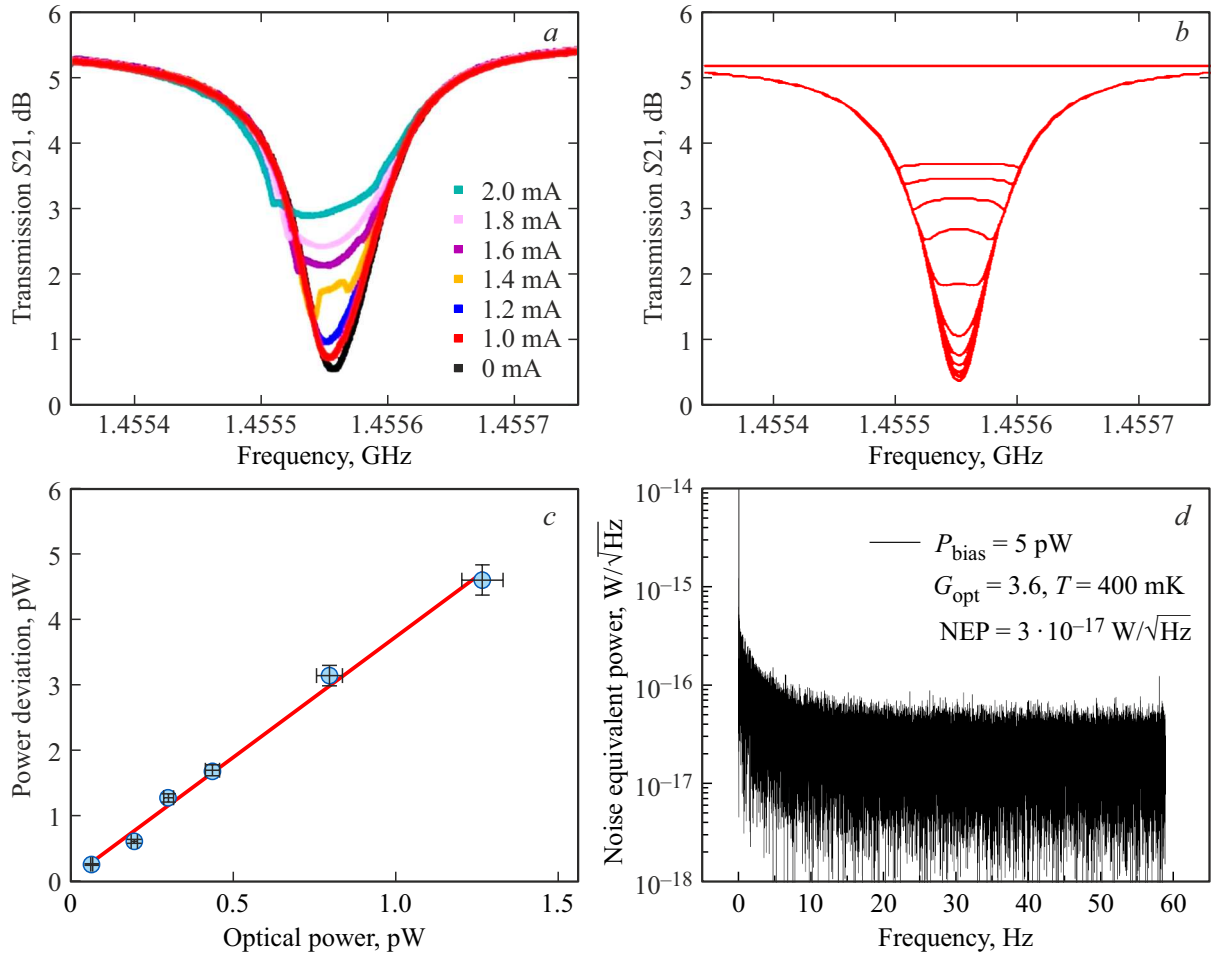

Figure 3. Characteristics of RFTES: *a*) illustration of the optical response in the form of a frequency scan for several values of the black-body heating current; *b*) calculation illustrating the mechanism of resonance curve distortion near resonance without involving the effect of critical current; *c*) dependence of the increase in the bias power at the detector output on the calculated power of black-body radiation (points), the linear trend has a coefficient of 3.6 (solid line); *d*) NEP as noise spectral density normalized to the microbridge input.

that such a film is a fairly effective absorber in the terahertz frequency range, and it can perform the function of a black body (BB). The temperature of the radiating surface of the BB (resistive film) was taken equal to the temperature of the sapphire substrate and was measured with a semiconductor thermometer glued to the back side (Fig. 2, *d*). The developed black-body emitter had characteristic thermal relaxation times from 1 to 10 s and was heated by a current of 0.2–2 mA passed through the film in the temperature range of 1–10 K. The test signal source was mounted to a copper rod that removed heat to the evaporation stage of the DR-200 refrigerator at temperature of 1 K, and was placed on the optical axis of the lens (Fig. 2, *c*) at a distance of $\sim$ 10 mm from its surface.

The high-frequency bias was applied to the chip through attenuators, which excluded the penetration of thermal noise 300 K. Two attenuators were used: 20 dB at the 55 K stage and 10 dB at the 3 K refrigerator stage. Buffer amplifiers with a total gain of $\sim$ 40 dB and a noise temperature reduced to the detector output of $\sim$ 20 K were installed at the stage 3 K: a niobium coaxial superconducting cable 2 mm in diameter and $\sim$ 0.5 m in length was used, which makes it possible to reduce the heat flux to the dilution stage. The transmittance of the circuit with the chip S_{21} was recorded by a vector network analyzer with an output power -44 dBm in the vicinity of the resonant frequency $\sim$ 1.5 GHz ($\pm$200 kHz).

3. Analysis of experimental data and discussion

Figure 3, *a* shows the change in the bias power $S_{21}(f)$ upon heating of the resistive film, which confirms the optical response of the bolometer to the broadband thermodynamic radiation of the BB. The distortion of the classical shape of the resonance curve, which occurs at significant levels of radiation and which is called „the crater“ in the literature, does not occur for all samples. For example, it was

not observed in studies [15,16], where bridges of smaller thickness (50 nm) with a lower critical superconducting transition temperature T_c were tested. Analogy with the classical TES is appropriate here, the operating point of which is automatically set to the operating resistance after reaching the critical current and the subsequent „jump“ to the resistive state. RFTES mode with critical current was analyzed in our works [10–13]. However, the calculation (Fig. 3, *b*) shows that such a characteristic can be explained qualitatively by the combination of high TCR $= dR/dT$ (TCR — thermal coefficient of resistance) and a high Q-quality of the resonator dZ/df, which leads to accelerated heating and a quick (on the frequency scale) transition to a stable regime at the bottom of the crater. These data are the solution of a simplified equation for the balance of received and dissipated power for the model dependence $R_b(T)$ using a fixed thermal conductivity $G \approx 10^{-11}$ W/K from the work [15]

$$P_{in} \cdot |S_{31}(f)| = G(T - T_{bath}), \qquad (1)$$

where P_{in} is the bias power supplied to the chip, $|S_{31}(f)|$ is the bias power transfer coefficient to the absorber $R_b(T(f))$, T_{bath} is substrate (cryostat) temperature. As a result of the numerical solution of this equation with respect to T on the grid of values f, we obtain the dependence $R_b(f)$, from which we determine $S_{21}(f)$ using the diagram from Fig. 1, *b*. Strictly speaking, the constant value G in (1) can only be used for small temperature changes. It is easy to see that the right side of equation (1) is an incremental excess of heat $(dP/dT) \cdot \Delta T$, which has limited applicability only for a small temperature difference and is used here only for a qualitative demonstration of the effect. For a more accurate calculation of the heat removal, either the integration of $\int_{T_{bath}}^{T} G(T)dT$, or the explicit expression $P \propto (T^6 - T_{bath}^6)$ should being used. The slight asymmetry of the entire dependence $S_{21}(f)$ is due to two factors. The first one is the bias power reflection from the coupler L_c. The phase jump in the resonator compensates for this reflection, which causes a slight improvement in transmission, i.e. skew $S_{21}(f)$ at a frequency just above resonance, and this effect does not depend on the characteristics of the bridge and is observed inter alia for MKID. Another factor may be thermal hysteresis, similar to what is observed in DC superconducting microbridges: the destruction current is always greater than the return current. The left edge of the crater $S_{21}(f)$ corresponds to the larger resonator current, the right edge corresponds to the return current (frequency scanning goes from left to right).

When determining the power of the optically supplied test signal P_{opt}, the Planck's nature of the spectrum and the fact that the slot antenna on the chip is polarized were taken into account, that is, the power of black-body radiation transmitted to the antenna is halved

$$P_{opt}(T_{BB}) = (A \cdot B)/2 \cdot \int_{f_1}^{f_2} hf\, df \Big/ \left(\exp\left(\frac{hf}{k_B T_{BB}}\right) - 1\right), \qquad (2)$$

where A is optical efficiency of the antenna, B is emissivity of the absorber film, h is Planck's constant, k_B is Boltzmann constant, T_{BB} is physical temperature of the absorber (of the sapphire substrate). The integration is carried out in the antenna matching frequency range with the bridge, which is selected in the atmospheric transparency window 600−700 GHz. The optical efficiency of the antenna, A, includes the optical losses in the lens, including absorption, reflection and diffraction losses, as well as mismatch between the bridge and the antenna. These parameters were estimated in the electromagnetic simulation program. The main lobe of diagram of double-slot antenna is directed into the substrate; reflections at the substrate boundary ($\varepsilon \approx 12$) with the lens ($\varepsilon \approx 10$), as well as on the spherical surface of the coated lens, are neglected. About 20% of the received power is lost in the back lobe of the lens antenna. Losses in the first-order side lobes of the frontal direction can be neglected, since they fall into the BB aperture with a diameter of 15 mm. Taking into account the matching of the antenna with the bridge ($S_{11} \approx -10$ dB), the value A was ~ 0.7. The emissivity B was estimated using the electromagnetic simulation program in the zero thickness metal approximation with a surface resistance of 1000 Ω/sq, and amounted to ~ 0.6. Thus, the transfer coefficient of black-body radiation to the microbridge was estimated to be 42%.

The thermal background power inside the cryostat in the antenna band is determined by the temperature of the internal radiation shields ($\sim 10^{-23}$ W at ~ 1 K) and can be neglected. The total power of the Planck emitter at the maximum temperature at ~ 10 K was estimated as ~ 100 pW. Direct infrared heating of the bolometer from the BB and heat transfer from the BB heater to the refrigerator thermal stabilization system (parasitic effects with a total power of ~ 2 mW) were studied in a separate experiment. The variation in the detector bias power caused by the heating of the BB with the lens covered with aluminum foil turned out to be at the level of transient fluctuations of system thermal controller by Lakeshore (~ 0.02 dB).

The normalized noise spectrum of the bolometer, normalized to its input (NEP), was calculated taking into account the thermal transfer coefficient of the detector. The RFTES bolometer is not a quadratic, but a linear power converter: the offset increment ΔP_{bias} at the output is related to the optical signal P_{opt} received by the antenna by means of a multiplier having the meaning of the gain. It is this property that makes it possible to use RFTES with an amplifier by the standard 50 Ohm, and not with a current amplifier, like a TES bolometer. The quadratic conversion of the power of the received signal into direct current/voltage does not occur

in the RFTES itself, but in the circuit of the final power recorder, after the buffer amplifier. The dimensionless power gain $\text{Gain} = \Delta P_{\text{bias}}/P_{\text{opt}}$ can be calculated using the bridge thermal power balance equation, P:

$$\begin{aligned}\text{Gain} &= (P_{\text{bias}}\Delta S_{21}/(\Delta P - P_{\text{bias}}\Delta S_{31}) \\ &= (P_{\text{bias}}(dS_{21}/dT)/(G - P_{\text{bias}} \cdot dS_{31}/dT). \qquad (3)\end{aligned}$$

In formula (3), the numerator is the change in bias power, and the denominator is the signal power on the bridge, which is the sum of the full increment ΔP minus the electrothermal feedback (ETF) power. The ETF effect occurs due to the change in the resistance of the bridge when it is heated by the signal. The right side of the relation (3) shows that the physical meaning of ETF is an addition to the removal or increment of heat, which depends on the sign of $dS_{31}(R)/dR$:

$$\text{ETF} = P_{\text{bias}} \frac{dS_{31}}{dT} = P_{\text{bias}} \frac{dS_{31}}{dR} \frac{dR}{dT}. \qquad (4)$$

Note that the ETF changes its sign depending on which of the ratios, $R(T) < R_s$ or $R(T) > R_s$, is satisfied for the selected detector operation mode (positive, PETF, near the superconducting state of the bridge or negative, NETF, respectively). It follows from (3) that too strong positive ETF can lead to infinite and even negative gain, which physically manifests itself as a jumpy dynamics at the edges of the aforementioned crater. In traditional TES bolometers, a low-resistance shunt is chosen from the $R_{\text{sh}} \ll R(T)$ condition and installed as close as possible to the detector to ensure unconditional stability — NETF. In the case of RFTES, the function of the shunt is performed by the resonator,more precisely, its impedance Z_s, which occurs at the discontinuity point where the bridge is connected.

It should be noted that RFTES stability is possible not only under the condition $R(T) > R_{\text{sh}}$. The fundamental difference of the high-frequency impedance reading is the smoother dependence of the superconducting transition $R(T)$, which we studied for hafnium in the works [14-16]. According to the theory of Matisse–Bardeen [17], the high-frequency impedance of the surface of a superconductor (thin film) near the critical temperature can be described qualitatively, somewhat simplifying, by two conduction channels. When cooled from the normal state, the presence of microwave photons prevents the abrupt appearance of superconducting carriers, the concentration of which remains low, and the resulting inductance leads to the emergence of a non-zero high-frequency potential. Because of this, normal electrons are involved in the current transfer and active losses occur, which gradually decrease as the lattice temperature decreases. This allows to fulfill the condition $G > \text{ETF} > 0$ for $R(T) \ll R_s$, which by formula (3) determines the stability S_{21}. The presence of active high-frequency losses at a temperature below the critical one is precisely the mechanism that makes it possible to realize the nonlinear impedance of microbridge with an electron gas. Note that high-frequency heating and critical current switching [10,13] seem to be competitive processes when RFTES enters the operating mode, which is interesting for further detailed study.

Figure 3, *c* shows the detector response to the optical signal, $\Delta P_{\text{bias}}(P_{\text{opt}})$, as separate points taken from Fig. 3, *a* at center frequency of the resonator. Applying a linear trend, we get $\text{Gain} = dP_{\text{bias}}/dP_{\text{opt}} \approx 3.6$ (~ 5.5 dB), which means the gain. According to the electrical circuit analysis, the presence of such amplification makes it possible to reduce the noise requirements of the buffer amplifier. The threshold sensitivity was determined using the fast Fourier transform. Discrete sampling from the amplitude noise track at the detector output, $P_{\text{bias}}(t)$, was transformed into the spectral density of fluctuations, $S_x(f)$ (Fig. 3, *d*). The frequency range of the resulting spectrum is determined, according to the Kotelnikov theorem, by the sampling time interval (8.5 ms), and its accuracy is determined by the total number of points of the noise track (100001 point). The selected spectrum range (0–60 Hz) lies in the frame rate of a standard video stream, which is important for the promising use of RFTES matrices in radio vision. The threshold sensitivity (Fig. 3, *d*) was determined by the standard method [22] as

$$\text{NEP}_{\text{exp}} = \frac{\sqrt{S_x}}{\text{Gain}},$$

where $S_x(f)$ is noise spectral density at the buffer amplifier input. From the data shown in Fig. 3, *d*, after mathematical averaging, it follows that the spectral density of the intrinsic noise of a bolometric receiving system, including a buffer semiconductor amplifier, has a plateau $(3 \pm 1) \cdot 10^{-17}$ W/Hz and flicker noise limit ~ 5 Hz.

Initial data analysis allows to assume that the flicker noise is the result of a combination of temporary instability of the refrigerator and industrial noise in the power supply circuit of the buffer amplifiers. Theoretical comparison of the measured and theoretical NEP was performed on the basis of taking into account the contributions of various noise sources:

$$\text{NEP}^2_{\text{tot}} = \text{NEP}^2_{\text{Johnson}} + \text{NEP}^2_{\text{photon}} + \text{NEP}^2_{\text{phonon}} + \text{NEP}^2_{\text{amp}}.$$

Amplifier with noise temperature TLNA $\approx$ 20 K gives

$$\text{NEP}_{\text{amp}} = \frac{\sqrt{0.5 k_{\text{B}} P_{\text{bias}} T_{\text{LNA}}}}{\text{Gain}} \approx 0.6 \cdot 10^{-17}\,\text{W}/\sqrt{\text{Hz}}.$$

The contribution of lattice thermal noise is characterized by phonon noise

$$\text{NEP}_{\text{phonon}} = \sqrt{4 k_{\text{B}} T^2 G_{e-\text{ph}}} \approx 0.9 \cdot 10^{-17}\,\text{W}/\sqrt{\text{Hz}}.$$

Here, the value $G_{e-\text{ph}} \approx 10^{-11}$ W/K obtained by extrapolation of the dependence $G_{e-\text{ph}}(T)$ from work [15], was used. The photon noise $\text{NEP}_{\text{photon}} \approx \sqrt{2 P_{\text{rad}} h f}$ has two independent components. The weak flux of terahertz

photons from the BB, which is determined by the temperature of the thermal armature (~ 1 K in dark mode), in the antenna band gives $\mathrm{NEP}_{\mathrm{photon1}} \approx 10^{-22}\,\mathrm{W}/\sqrt{\mathrm{Hz}}$, and this component can be neglected. The second component is the bias photon flux at 1.5 GHz at -79 dBm, giving $\mathrm{NEP}_{\mathrm{photon2}} \approx 0.5 \cdot 10^{-17}\,\mathrm{W}/\sqrt{\mathrm{Hz}}$. Since the physical temperature of the bridge is much lower than the noise temperature of the amplifier, the contribution of Johnson noise in the microbridge can be neglected. The obtained value of $\mathrm{NEP}_{\mathrm{tot}}$ gives the theoretical limit of sensitivity for the experimental sample $\sim 1.5 \cdot 10^{-17}\,\mathrm{W}/\sqrt{\mathrm{Hz}}$. With cold sky background radiation in the stratosphere at a level of 8–10 K in the transparency window of 600–700 GHz, the RFTES photon load will degrade the threshold signal to $\mathrm{NEP}_{\mathrm{photon1}} \approx 3 \cdot 10^{-17}\,\mathrm{W}/\sqrt{\mathrm{Hz}}$, which exceeds the intrinsic noise of the investigated detector and allows it to be used as an effective tool for stratospheric platforms.

4. Conclusion

The performed studies of the optical sensitivity confirm the effectiveness of the RFTES bolometer concept, which is based on the use of the active component of the high-frequency nonlinear impedance of the superconducting bridge with electron gas. The optical sensitivity of the RFTES bolometer obtained in the experiment, which is only 1.5 times lower than the theoretical value, can be considered as a promising result. The method for determining the NEP detector by the calculated parameters of the radiation of the BB should not be considered precise. It is possible that the optical signal used in the analysis is overestimated, and the NEP of the system is actually closer to the theoretical value. In passing to electron-beam lithography, the volume of electron gas in the bridge can be reduced by a factor of 300–400 times and the critical temperature by a factor of 2–3 times by reducing the film thickness to about 20–30 nm. On the basis of the conducted studies, one can be optimistic about the possibility of obtaining NEP at the level of $\sim 10^{-20}\,\mathrm{W}/\sqrt{\mathrm{Hz}}$. The authors hope that this study may open the way to the creation of a new generation of practical ultra-high-sensitivity detectors and imaging arrays with frequency-selective multiplexing.

Funding

The study was performed entirely at the site of NUST MISiS and was supported by grants of NUST MISiS No. K2-2020-016, RSF No. 17-19-01786 and RFBR No. 20-37-90094.

Conflict of interest

The authors declare that they have no conflict of interest.

References

[1] J. Clarke, P.L. Richards, N.H. Yeh. Appl. Phys. Lett. **30**, *12*, 664 (1977).
[2] S.F. Lee, J.M. Gildemeister, W. Holmes, A.T. Lee, P.L. Richards. Appl. Opt. **37**, *16*, 3391 (1998).
[3] D.K. Day, H.G. LeDuc, B.A. Mazin, A. Vayonakis, J. Zmuidzinas. Nature **425**, *6960*, 817 (2003).
[4] J. Zmuidzinas. Annu. Rev. Condens. Matter Phys. **3**, 169 (2012).
[5] B.S. Karasik, W.R. McGrath, H.G. LeDuc, M.E. Gershenson. Supercond. Sci. Technol. **12**, *11*, 745 (1999).
[6] B.S. Karasik, D. Olaya, J. Wei, S.V. Pereverzev, M.E. Gershenson, J.H. Kawamura, W.R. McGrath, A.V. Sergeev. IEEE Trans. Appl. Supercond. **17**, *2*, 293 (2007).
[7] L.S. Kuzmin, A.L. Pankratov, A.V. Gordeeva, V.O. Zbrozhek, V.A. Shamporov, L.S. Revin, A.V. Blagodatkin, S. Masi, P. de Bernardis. Commun. Phys. **2**, 104 (2019).
[8] S.V. Shitov. Technical Phys. Lett. **37**, *10*, 932 (2011).
[9] A. Kuzmin, S.V. Shitov, A. Scheuring, J.M. Meckbach, K.S. Il'in, S. Wuensch, A.V. Ustinov, M. Siegel. IEEE Trans. Terahertz Sci. Technol. **3**, *1*, 25 (2013).
[10] A.A. Kuzmin, S.V. Shitov, A.V. Ustinov. ZhTF **84**, *1*, 139 (2014) (in Russian).
[11] S.V. Shitov, N.N. Abramov, A.A. Kuzmin, M. Merker, M. Arndt, S. Wuensch, K.S. Ilin, E.V. Erhan, A.V. Ustinov, M. Siegel. IEEE Trans. Appl. Supercond. **25**, *3*, 12 (2014).
[12] S.V. Shitov, A.A. Kuzmin, M. Merker, V.I. Chichkov, A.V. Merenkov, A.B. Ermakov, A.V. Ustinov, M. Siegel. IEEE Trans. Appl. Supercond. **27**, *4*, 1 (2017).
[13] A.A. Kuzmin, M. Merker, S.H. Wuensch, M. Siegel, A.D. Semenov, S.V. Shitov, A.V. Ustinov. Appl. Phys. Lett. **111**, *4*, 042601 (2017).
[14] A.V. Merenkov, V.I. Chichkov, A.B. Ermakov, A.V. Ustinov, S.V. Shitov. IEEE Trans. Appl. Supercond. **28**, 7 (2018).
[15] A.V. Merenkov, S.V. Shitov, V.I. Chichkov, A.B. Ermakov, T.M. Kim, A.V. Ustinov. Tech. Phys. Lett. **44**, *7*, 581 (2018).
[16] A.V. Merenkov, V.I. Chichkov, A.V. Ustinov, S.V. Shitov. IOP Conf. Ser.: J. Phys. **1182**, 012009 (2019).
[17] C. Mattis, J. Bardeen. Phys. Rev. **111**, *2*, 412 (1958).
[18] B.L. Altshuler, A.G. Aronov. Modern Problems. Condens. Matter Sci. **10**, 1 (1985). ISSN 0167-7837,
[19] A.F. Andreev. Sov. Phys. JETP **19**, *5*, 1228 (1964).
[20] B.S. Karasik, R. Cantor. Appl. Phys. Lett. **98**, *19*, 193503 (2011).
[21] http://www.tydexoptics.com/ru/
[22] E.L. Dereniak, G.D. Boreman. Infrared Detectors and System. John Wiley & Sons, N.Y. (1996).